Role of gas density in the stability of single-bubble sonoluminescence

L. Yuan,[1] C. Y. Ho,[2] M.-C. Chu,[2] and P. T. Leung[2]
[1]*State Key Laboratory of Scientific and Engineering Computing and Institute of Computational Mathematics, Academy of Mathematics and System Sciences, Chinese Academy of Sciences, Beijing 100080, China*
[2]*Department of Physics, The Chinese University of Hong Kong, Shatin, New Territories, Hong Kong, China*
(Received 14 December 2000; published 27 June 2001)

Recent full hydrodynamic simulations of a sonoluminescing bubble interior have shown that the bubble content is compressed to a very dense state during the violent collapse. In this paper, we numerically studied the shape stability of a radially oscillating gas bubble by using Hilgenfeldt *et al.* theoretical model with corrections taking into account the gas density effect. Our results show that gas density variations not only significantly suppress the Rayleigh-Taylor instability, but also enhance the threshold of the parametric instability under sonoluminescence conditions.

DOI: 10.1103/PhysRevE.64.016317 PACS number(s): 78.60.Mq, 43.25.+y, 44.10.+i, 47.20.Ma

I. INTRODUCTION

Since the first report of single bubble sonoluminescence (SBSL) by Gaitan *et al.* [1], the phenomenon has been extensively and carefully studied, and numerous models have been proposed to explain its mechanism [2]. Recent measurements of the light pulse of SBSL revealed that the full widths at half maximum range from 40 to 380 ps in various experimental conditions [3] and put constraints on models. However, they still seem to be consistent with a wide range of hydrodynamic scenarios including shock wave [2,4], continuous compression wave [5,6], or even adiabatic heating of the bubble content [7,8]. Aside from the light-emitting mechanism and related hydrothermal scenarios, another remarkable feature of SBSL is that it can be stable for millions of cycles. In most of the previous models, a spherically symmetric collapse is assumed, even though this seeming contradicts the long known fact that the spherical shape of oscillating gas bubbles can be unstable [9,10].

The remarkable stability of SBSL have been explained partially by several authors based on, most notably, the argon-rectification hypothesis [11] and the analysis of shape and diffusive instabilities [12–14]. These works have established that stable SBSL only occurs in a narrow parameter window of large driving pressure amplitude and low dissolved gas concentration, resulting from instabilities of shape, diffusion, and chemical reactions for molecular gases. However, their studies about the regions in which stable SBSL may exist map out a stability threshold for the equilibrium bubble radius (R_0) that lies well below those found in experiments [15]. The boundary layer approximation (BLA) used in these studies for evaluating the destabilizing role of the vorticity field has been controversial [16,17]. Recently Hao and Prosperetti [18] conducted a full numerical simulation considering the viscous nonlocal effects to compare with the BLA. While noting a satisfactory agreement at low driving pressure amplitudes $P_a<0.6-0.7$ bars, they found that the BLA underpredicted the parametric instability (PI) threshold at $P_a>1$ bar. As regard to another type of shape instability, namely, the short time-scale Rayleigh-Taylor (RT) instability, there are no agreed threshold up to now and discrepancies about whether the RT instability in the main collapse of single sonoluminescing bubbles is a major concern exist even in very recent studies [19,20]. Therefore, further theoretical clarifications are desirable.

The objective of this paper is to improve the shape stability analysis of a radially oscillating gas bubble by considering the variation of the gas density inside the bubble and to evaluate its role in stable SBSL. This is motivated by some full numerical simulations of the bubble interior [21]. Figure 1 shows typical density profiles at the moment of minimum bubble radius $R_{\min}$ for three driving pressure amplitudes P_a calculated using our full hydrodynamic model [6] and a realistic equation of state [22] taking into account the ionization processes in the bubble interior. The average density of the bubble content becomes comparable to or even larger than that of the surrounding water at high driving pressure. A direct effect of this is to reduce the difference between the gas density ρ_g and the liquid density ρ_w, which is expected to suppress the RT instability. During the course of our investigation, we note that recently Augsdörfer *et al.* [19] also studied the gas density effect in the spherical RT instability

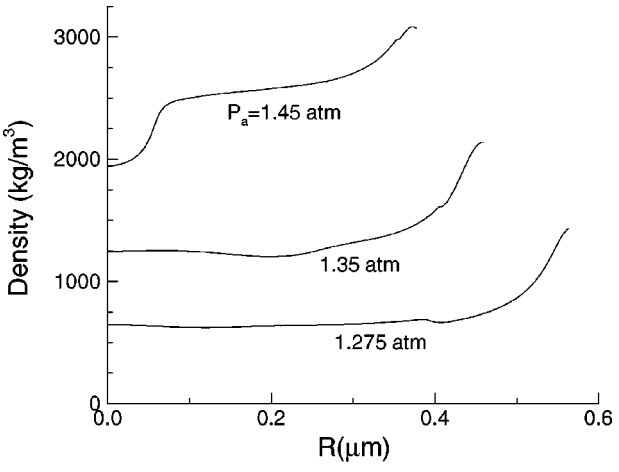

FIG. 1. Calculated spatial profiles of gas density of an argon bubble at the moment when the bubble radius attains its minimum at $P_a=1.275$, 1.35, and 1.45 atm, respectively. The driving sound has a frequency $f=26.5$ kHz, and the bubble equilibrium radius is $R_0=4.5$ μm.

by exemplifying its influence on the coefficients of the equation for the distortion amplitude. Our work differs from Ref. [19] mainly in that we use a different approach; specifically, we track the evolution of initial distortions rather than that of *ad hoc* thermal fluctuations [19]. Our approach is simpler, computationally less intensive, and able to make use of the Floquet theory of Hill's equation for determining the parametric instability (see the details given in Sec. II A). Another difference is that we adopt a different form of the Rayleigh-Plesset equation (RP) that leads to stronger collapse. The resulting higher density seems closer to that obtained from full hydrodynamic simulations. Furthermore, we studied also the effect of gas density variations on the parametric instability.

II. BUBBLE DYNAMICS

A. Shape stability

We concentrate on pure argon bubbles for which no chemical instability can occur, and we ignore the translational movement of the bubble for which no Bjerknes force instability will appear. The later assumption is justified for $P_a \leqslant 1.6$ atm [23]. To examine the regime where stable SBSL exists in the experimental control parameters $(P_a, f, c_\infty/c_0, T_\infty)$, where $f=\omega/2\pi$ is the external driving frequency, c_∞ is the gas concentration far away from the bubble, c_0 is the saturation concentration, and T_∞ is the ambient temperature, we follow Hilgenfeldt *et al.* approach [12] to analyze parametric and diffusive instabilities, but starting from Prosperetti's formula [24] that takes into account of the viscosity of the surrounding water and the density of the bubble content.

Let the bubble radius be perturbed to $R(t)+a_n(t)Y_n(\theta,\phi)$, where R is the undistorted bubble radius, $a_n(t)$ is the distortion amplitude, and Y_n is a spherical harmonics of degree n. In the linear regime, the dynamical equation for $a_n(t)$ can be obtained from Eqs. (17), (23), and (25) in [24] by setting $\mu_1=0$, retaining $\rho_1(\rho_g)$ and $\rho_2(\rho_w)$, and adopting the BLA [12]:

$$\ddot{a}_n + B_n(t)\dot{a}_n + A_n(t)a_n = 0 \tag{2.1}$$

with

$$B_n(t) = \frac{3\dot{R}}{R} + \frac{\left[-\beta_n + \frac{n(n+2)^2}{1+2\delta/R}\right]\frac{2\nu}{R^2}}{1+\frac{n+1}{n}\frac{\rho_g}{\rho_w}},$$

$$A_n(t) = \left\{\left[\frac{(n+1)(n+2)}{n}\frac{\rho_g}{\rho_w} - (n-1)\right]\frac{\ddot{R}}{R} + \frac{\beta_n\sigma}{\rho_w R^3} + \left[\beta_n - \frac{n(n-1)(n+2)}{1+2\delta/R}\right]\frac{2\nu\dot{R}}{R^3}\right\} \Bigg/ \left(1+\frac{n+1}{n}\frac{\rho_g}{\rho_w}\right), \tag{2.2}$$

where $\beta_n=(n-1)(n+1)(n+2)$, dots denote time derivatives, ν,σ are the kinematic viscosity and surface tension of the liquid, and δ is the boundary layer thickness. There are several observations on Eq. (2.2): (i) if the density ratio $\rho_g/\rho_w=0$, one recovers the formula of [12]; (ii) although a finite density ratio may reduce the magnitude of the second term in $B_n(t)$ (the damping), it changes the contribution of $\ddot{R}$ in $A_n(t)$ far more significantly [19]. The net effect is to enhance shape stability, which will be shown later; (iii) the boundary layer thickness $\delta=\min(\sqrt{\nu/\omega}, R/2n)$ proposed in [12,13], though reasonable qualitatively, notably overestimates the destabilizing role of the vorticity field quantitatively at both low and high driving amplitudes [16,18]. In view of the complexity of accurate methods for evaluating the viscous nonlocal effects [18], and because our test results show that the RT instability is hardly affected whether the BLA is used, we prefer to consider the limiting case of a thin layer associated with the least destabilizing effect of the vorticity field, namely $\delta\to 0$. However, we also use different δ to demonstrate its impact on the PI threshold.

Three kinds of shape instabilities hidden inside Eq. (2.1) were distinguished by Hilgenfeldt *et al.* [12], namely, the parametric, the RT and the afterbounce, acting on different time scales and different P_a-R_0 parameter regions. We here focus on the first two kinds. If $R(t)$ and thus $A_n(t)$ and $B_n(t)$ are periodic with period T, Eq. (2.1) is a Hill's equation and a pure parametric instability can be rigorously analyzed. The Floquet transition matrix is numerically computed by evolving small perturbations through one period T [12]. Parametric instability occurs whenever the maximal eigenvalue of the Floquet transition matrix of Eq. (2.1) is larger than one. As a result of incremental search in the P_a-R_0 space, we obtain a PI borderline that divides the stable and unstable domains.

The RT instability happens in a short time scale when the bubble rebounds from the minimum bubble radius. Up to now, there is no established quantitative threshold for the RT instability [2,12,16]. In the literature, there is basically two approaches to study the RT instability numerically. One is to add either a random displacement to the distortion $a_n(t)$ after each integration time step [12] or a random force of molecular fluctuations [19] to the right-hand side of Eq. (2.1) during the whole cycle, another is to compute the amplification factor of an initial distortion of microscopic sizes only during the primary collapse [20]. Our experience shows that the latter approach is computationally cheaper, and it is thus used in this paper. We define the primary collapse as the period from the moment of maximum bubble radius $t_{R_{\max}}$ when an initial perturbation $(a_n^0, \dot{a}_n^0)$ starts to grow to the moment in the first rebounce when the distortion $a_n(t)$ ceases to grow. We adopt the approximate criterion [12] that the distortion can overwhelm the bubble radius $R(t)$ within the collapse stage

$$\max_{\{t_{R_{\max}} < t < t_{R_{\min}} + t_{\mathrm{RT}}\}} \left(\frac{|a_n(t)|}{R(t)}\right) \geqslant 1, \tag{2.3}$$

where $t_{R_{\min}}$ is the moment of minimum bubble radius, and

t_{RT} is set to 10 ns to cover the moment when the distortion ceases to grow. It should be emphasized that both the displacement and velocity of an initial perturbation will affect the location of the RT borderline determined by Eq. (2.3). Since our main concern is to study the effects of the density ratio under otherwise the same conditions, we assume that when an initial perturbation of $a_n^0=10$ nm, $\dot{a}_n^0=0$ can grow to overwhelm the bubble radius $R(t)$, the RT instability will disrupt the bubble. In view of the fact that the 10 nm size is less than 1% R_0 and $\dot{a}_n^0$ has not been taken into account, we think that the above initial perturbation is typical of practical imperfections that may occur. Our numerical results show that the calculated RT borderline lies just above the experimental upper boundary in P_a with very low gas concentration [15]. Even though the exact position of the predicted RT threshold is affected by the size of a_n^0, the amplification factor $a_n(t)/a_n^0$ is independent of a_n^0 because Eq. (2.1) is linear. As we will show in Sec. III, the density ratio has a significant effect on the stability threshold.

B. Diffusive stability

To obtain a phase diagram with experimental control parameters, we also consider diffusive instability according to Fyrillas and Szeri [25]. The equilibrium radius follows from the dynamical condition that the mass outflow and inflow during a driving cycle are balanced

$$\frac{c_\infty}{c_0}=\frac{\langle p(t)\rangle_{t,4}}{P_0}, \tag{2.4}$$

where the weighted time average $\langle\ \rangle_{t,4}$ is defined as

$$\langle f(t)\rangle_{t,4}=\frac{\int_0^T f(t)R^4(t)dt}{\int_0^T R^4(t)dt}. \tag{2.5}$$

Thus we can plot $\langle p\rangle_{t,4}/P_0 \sim R_0$ for different P_a. The intersections of a constant c_∞/c_0 line with the $\langle p\rangle_{t,4}/P_0 \sim R_0$ curve correspond to equilibrium points, and a diffusively stable point is indicated by $d\langle p(t)\rangle_{t,4}/dR_0>0$.

C. The Rayleigh-Plesset equation

To provide Eqs. (2.1) and (2.4) with $R(t)$ and $p(R,t)$, we use the RP equation that describes the dynamics of the bubble wall. A simpler form [2,12,14] is used:

$$R\ddot{R}+\frac{3}{2}\dot{R}^2=\frac{1}{\rho_w}[p(R,t)-P_s(t)-P_0]+\frac{R}{\rho_w c_w}\times\frac{d}{dt}[p(R,t)-P_s(t)]-4\nu\frac{\dot{R}}{R}-\frac{2\sigma}{\rho_w R}, \tag{2.6}$$

where $P_s(t)=-P_a\sin(\omega t)$ is the acoustic driving pressure. The gas pressure and temperature inside the bubble vary according to

$$p[R(t)]=\left(P_0+\frac{2\sigma}{R_0}\right)\left(\frac{R_0^3-h^3}{R^3-h^3}\right)^\gamma, \tag{2.7}$$

$$T[R(t)]=T_\infty\frac{(R_0^3-h^3)^{\gamma-1}}{(R^3-h^3)^{\gamma-1}}, \tag{2.8}$$

and the gas density ρ_g is computed from

$$p=\frac{\rho_g R_g T}{1-b\rho}, \tag{2.9}$$

where $h=R_0/8.86$ is the hard core van der Waals radius for argon bubbles, R_g is the gas constant, and b is the excluded van der Waals hard core volume, and for argon $b=0.032\,19l/\text{mole}$. The polytropic exponent γ includes the effects of heat transfer between the bubble and the liquid in a simplified way. In doing so, $\gamma=1$ is used for radii larger than R_0 and $\gamma=5/3$ is used for smaller radii [2]. We want to compare with the experiments of Holt and Gaitan [15], and hence other parameters are $P_0=1$ atm, $T_\infty=20\,^\circ$C, $f=20.6$ kHz, $\sigma=0.0728$ kg/s^2, $\nu=1.008\times10^{-6}$ m^2/s, $\rho_w=998$ kg/m^3, $c_w=1483$ m/s.

III. RESULTS AND DISCUSSIONS

We study the parameter range 0.65 atm$\leqslant P_a\leqslant$1.5 atm, 1 μm$\leqslant R_0\leqslant$20 μm. The computational resolution in the P_a-R_0 parameter space is $\Delta P_a=0.025$ atm, $\Delta R_0=0.25$ μm. The quadrupole mode ($n=2$) is most unstable for $R_0<10$ μm and is considered here. Before discussing the effects of gas density, let us first show how the boundary layer thickness δ and polytropic exponent γ affect the numerical results.

Figure 2 shows the borderlines of the parametric and RT instabilities in the P_a-R_0 parameter space obtained using various δ. Below the PI line the bubble is parametric stable. To the left of the RT line the bubble is RT stable. As δ increases from $\delta=0$ to $\min(\sqrt{\nu/\omega},R/2n)$ the location of the maximum R_0 deviates more from the experimental threshold [15], and the margin between $\delta=0$ and $\delta=\min(\sqrt{\nu/\omega},R/2n)$ can be nearly 2 μm for $P_a>1.1$ atm. We note the quantitative agreement of the location of the PI line for $\delta=\min(\sqrt{\nu/\omega},R/2n)$ between the present result and Fig. 13 in Ref. [18]. The result reflects the earlier conclusion that the viscous damping is notably underestimated by the BLA [18]. However, the RT line is hardly affected by the choice of δ. Figure 3 shows the influence of the polytropic exponent on the predicted stability thresholds. The difference in the PI threshold becomes obvious at lower driving amplitudes, with the threshold from the full isothermal model being the most left and that from the full adiabatic one being the most right. However, the difference is very small for $P_a>1.2$ atm that is more relevant to SBSL. The trend in the PI threshold is the same as those predicted by Hao and Pros-

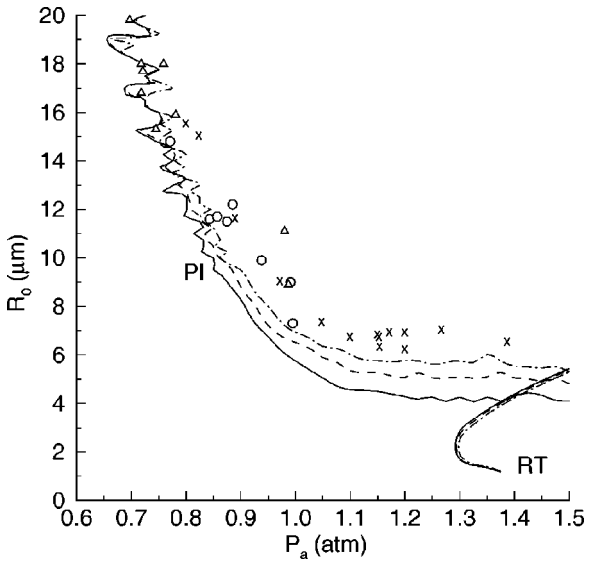

FIG. 2. Shape stability boundaries of the $n=2$ mode in the P_a-R_0 parameter space for an argon bubble driven at $f=20.6$ kHz. The PI and RT lines denote the parametric and RT instability borderlines respectively, obtained using various boundary layer thickness. Solid lines: $\delta=\min(\sqrt{\nu/\omega},R/2n)$; dashed lines: $\delta=0.1R$; dash-dotted lines: $\delta=0$. Symbols represent stability thresholds from experiments by Holt and Gaitan [15], where ○ stands for $n=2$ mode, △ for $n=3$ mode, and × for unknown shape mode.

peretti [18]. The RT instability threshold is also affected by the polytropic exponent, with the full adiabatic model being the most stable. The margin between different polytropic exponents will be compared to that caused by gas density

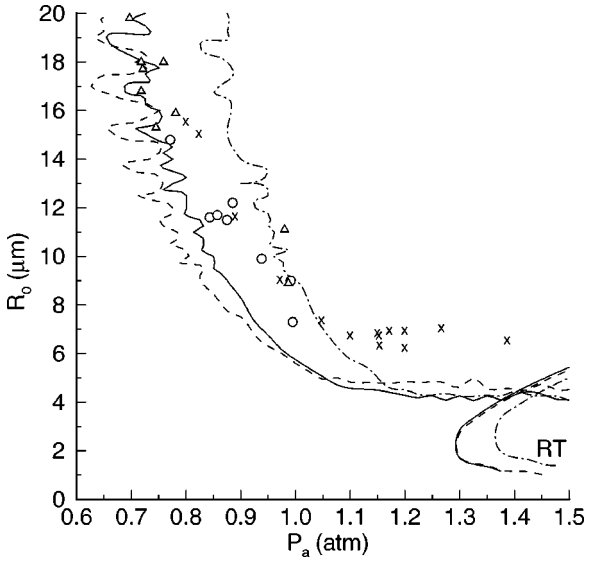

FIG. 3. Comparison between the shape stability boundaries of the $n=2$ mode as computed with various polytropic exponents and the same boundary layer thickness $\delta=\min(\sqrt{\nu/\omega},R/2n)$. Solid lines: mixed isothermal-adiabatic model of this paper; dashed lines: full isothermal model ($\gamma=1$); dash-dotted lines: full adiabatic model ($\gamma=5/3$). Symbols represent stability thresholds from experiment [15] as explained in Fig. 2.

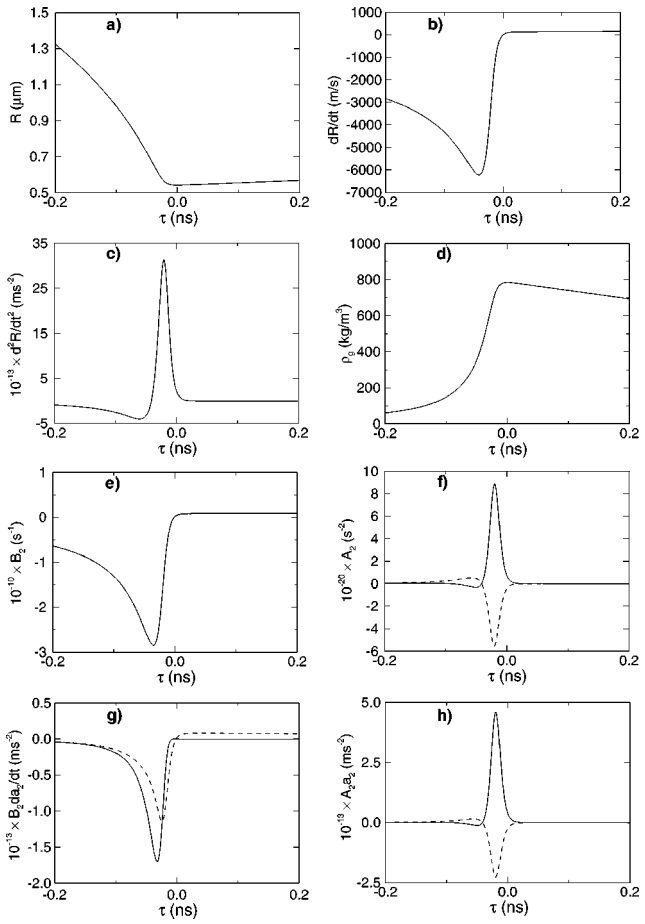

FIG. 4. (a)–(d) show the time development of the radius, velocity, and acceleration of the bubble during the brief stage of collapse and rebounce, for $R_0=4$ μm and $P_a=1.4$ atm. $\tau=0$ corresponds to the moment of minimum bubble radius. (e) and (f) show comparison between with considering (solid) and without considering the gas density (dashed) for the dynamics of $B_2(t)$ and $A_2(t)$ in Eq. (2.1). (g) and (h) show the magnitudes of $B_2(t)\dot{a}_2(t)$ and $A_2(t)a_2(t)$ respectively.

variations later in Fig. 6. The conclusions from the above comparisons are: (i) The choice of δ affects the PI threshold significantly but not the RT instability threshold; (ii) The choice of the polytropic exponent affects the PI threshold only for $P_a<1$ atm, and it is essential to treat thermal conduction properly at the low P_a regime. The following discussions are based on the results obtained using $\delta=0$ and the simplified polytropic exponent as described in Sec. II C.

We now turn to discuss the effect of the gas density on the shape stability. In most periods of a cycle or at low P_a, the density ratio ρ_g/ρ_w is negligible. But for larger P_a and when the bubble radius is close to its minimum, it is nontrivial. The density ratio will have important effects on $A_n(t)$ in Eq. (2.2) and hence may change the contribution of $\ddot{R}$, a dominant factor in the RT instability. Figures 4(a)–4(d) show the time history of the bubble's radius, velocity, acceleration, and gas density respectively during the final stage of collapse and rebounce, and Figs. 4(e)–4(h) show the dynamics of several quantities in Eq. (2.1) similar to those in Fig. 2 of

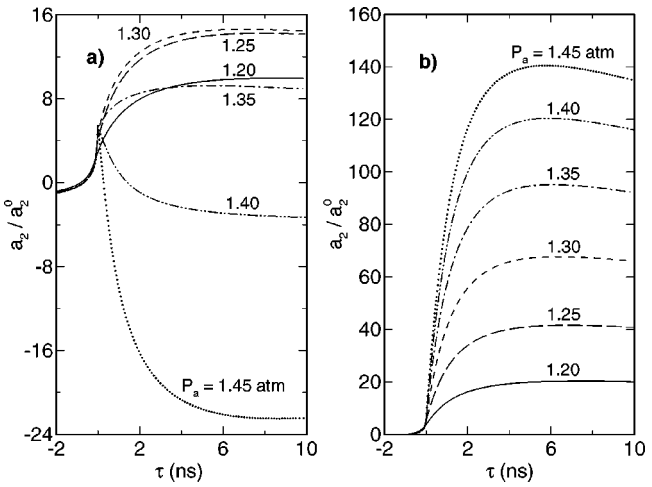

FIG. 5. Time history of the normalized distortion amplitude of the $n=2$ mode in the vicinity of minimum bubble radius with (a) considering and (b) without considering the gas density. In (a) the RT instability is strongly suppressed. The driving pressure amplitudes are marked in the plot, $R_0=4$ μm, and other conditions are the same as Fig. 2.

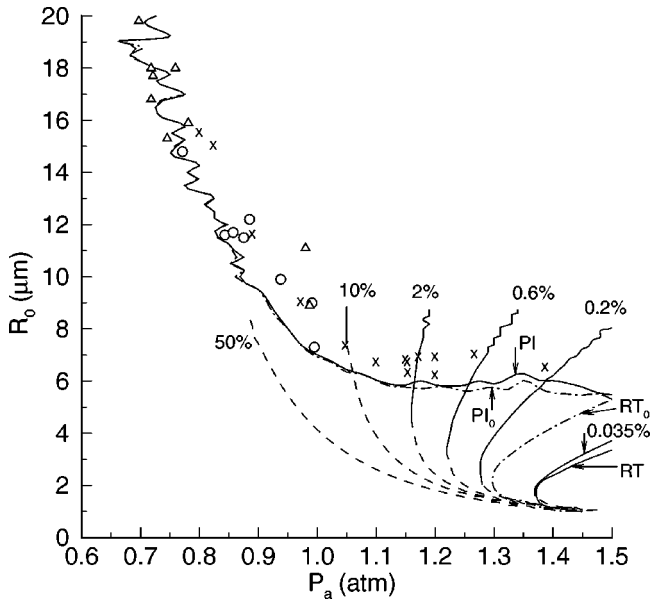

FIG. 6. Phase diagram in the P_a-R_0 parameter space for the case as in Fig. 2. The PI and PI_0 lines are the parametric instability borderlines with and without density ratio respectively, while the RT and RT_0 lines are the corresponding Rayleigh-Taylor instability borderlines. The solid parts of diffusive equilibria represent stable equilibria $R_0(P_a)$, and the dashed parts are unstable. Symbols indicate experimental data [15] as explained in Fig. 2.

[19]. Although $B_n(t)$ is slightly affected by the gas density [actually no difference can be seen in Fig. 4(e)], the value of $A_n(t)$ is greatly altered and even becomes positive [Fig. 4(f)], where a postive $A_n(t)$ causes the distortion to decrease. Our results agree qualitatively with those of Augsdörfer *et al.* [19] but show stronger effect of the gas density variation due to the use of a different form of the RP equation. In Fig. 5, we compare the evolution of a_2/a_2^0 near the minimum bubble radius between with and without the gas density. The figure shows that when the effect of the gas density is included, the originally intensive RT instability is strongly suppressed: for $P_a \leqslant 1.35$ atm, the maximal values of $a_2(t)/a_2^0$ are now much smaller than those without considering the gas density, while at $P_a=1.4$ atm, the distortion a_2/a_2^0 even reverts its sign and increases negatively. However, at still higher $P_a=1.45$ atm, the distortion increases negatively and intensive development of the RT instability again occurs. Thus there is a narrow regime of $P_a=1.35\sim1.4$ atm (for $R_0=4$ μm) where the RT instability is weakened.

As we use Floquet's theorem to determine the PI threshold, and the deformation of a perturbation depends on the stage of the violent collapse, it is expected that the PI threshold will also be affected by the gas density. Therefore we further studied the effect of the gas density on both the PI and the RT instability thresholds in the P_a-R_0 parameter space. Figure 6 shows the borderlines of the shape instabilities and diffusive equilibria at several dissolved gas concentrations. The fixed c_∞/c_0 line corresponds to diffusive equilibrium, where the parts with positive slope ($\partial R_0/\partial P_a>0$) are diffusively stable and vice versa. For example, when the gas concentration is 0.2%, its stable branch intersects with the PI line as P_a increases, thus forming a stable line segment on which stable SBSL occurs. As the gas concentration reduces further, say to 0.035%, a diffusively stable branch will intersect with both the PI and RT lines. Thus the RT instability sets an upper limit on the increase of the SL intensity by degassing the liquid. We note that the PI line lies about $0.2\sim0.5$ μm above the PI_0 line for $P_a=1.25\sim1.4$ atm, implying that the PI is also suppressed to some extent by gas density variations inside the bubble.

The results in Fig. 6 also allow us to compare the effect of the gas density on the shape instabilities with that caused by other factors such as the polytropic exponent and the liquid viscosity. It can be seen that the onset of the RT instability occurs at $P_a\approx1.3$ atm when the gas density is neglected (the RT_0 line). However, the onset of the RT instability can be delayed towards $P_a\approx1.37$ atm when the gas density is considered (the RT line). For increased bubble sizes, e.g., $R_0\geqslant3$ μm, the delay in the driving pressure amplitude can be 0.2 atm. The margin between the RT line and the RT_0 line is quite wide compared to that caused by the polytropic exponent as shown in Fig. 3. The relative distortion a_2/R on the RT_0 line is one, but is now less than 0.2 when the gas density is considered, implying better sphericity. The RT_0 line could be shifted to around the position of the RT line if the water viscosity is artificially increased to three times as large as its standard value. All these indicate that the effect of gas density variation is significant.

IV. CONCLUSION

We have revealed the nontrivial role of the gas density variation in stabilizing the bubble shape against the Rayleigh-Taylor and parametric instabilities in the SBSL parameter region. We show that a perturbation of the size of several nanometers can lead to strong RT instability that may destroy a bubble if gas density variations are neglected while

including them can suppress the RT instability significantly and reduce the parametric instability to some extent. It seems that the violent compression of an SL bubble that leads to light emission also stabilizes the bubble shape. Nevertheless, further study free from the spherical symmetry assumption is necessary in the future.

ACKNOWLEDGMENTS

We are thankful for the support of the state key program for developing basic sciences in China G1999032801, a Hong Kong Research Grants Council Grant No. CUHK 312/96P, and a Chinese University Direct Grant No. ID 2060093.

[1] D. Gaitan *et al.*, J. Acoust. Soc. Am. **91**, 3166 (1992).
[2] B. Barber *et al.*, Phys. Rep. **281**, 65 (1997), and references therein.
[3] B. Gompf, R. Günther, G. Nick, R. Pecha, and W. Eisenmenger, Phys. Rev. Lett. **79**, 1405 (1997); R. Hiller, S. Putterman, and K. Weninger, *ibid.* **80**, 1090 (1998); M. Moran and D. Sweider, *ibid.* **80**, 4987 (1998).
[4] W. Moss, D. Clarke, and D. Young, Science **276**, 1398 (1997).
[5] V. Vuong and A. Szeri, Phys. Fluids **8**, 2354 (1996).
[6] L. Yuan, H. Cheng, M.-C. Chu, and P.T. Leung, Phys. Rev. E **57**, 4265 (1998); H.Y. Cheng, M.-C. Chu, P.T. Leung, and L. Yuan, *ibid.* **58**, R2705 (1998).
[7] S. Hilgenfeldt, R. Grossmann, and D. Lohse, Nature (London) **398**, 403 (1999); Phys. Fluids **11**, 1318 (1999).
[8] K. Yasui, Phys. Rev. Lett. **83**, 4297 (1999).
[9] M. Plesset, J. Appl. Phys. **25**, 96 (1954).
[10] A. Prosperetti, J. Acoust. Soc. Am. **101**, 2003 (1997); T. Lepoint *et al.*, *ibid.* **101**, 2012 (1997).
[11] D. Lohse, M. Brenner, T. Dupont, S. Hilgenfeldt, and B. Johnston, Phys. Rev. Lett. **78**, 1359 (1997).
[12] S. Hilgenfeldt, D. Lohse, and M. Brenner, Phys. Fluids **8**, 2808 (1996); **9**, 2462(E) (1996).
[13] M. Brenner, D. Lohse, and T. Dupont, Phys. Rev. Lett. **75**, 954 (1995); M. Brenner *et al.*, *ibid.* **76**, 1158 (1996).
[14] R. Löfstedt, K. Weninger, S. Putterman, and B. Barber, Phys. Rev. E **51**, 4400 (1995).
[15] R. Holt and D. Gaitan, Phys. Rev. Lett. **77**, 3791 (1996); D. Gaitan and R. Holt, Phys. Rev. E **59**, 5495 (1999).
[16] S. Putterman and P. Roberts, Phys. Rev. Lett. **80**, 3666(C) (1998).
[17] M. Brenner, T. Dupont, S. Hilgenfeldt, and D. Lohse, Phys. Rev. Lett. **80**, 3668(C) (1998).
[18] Y. Hao and A. Prosperetti, Phys. Fluids **11**, 1309 (1999); A. Prosperetti and Y. Hao, Philos. Trans. R. Soc. London, Ser. A **357**, 203 (1999).
[19] U. Augsdörfer, A. Evans, and D. Oxley, Phys. Rev. E **61**, 5278 (2000).
[20] V. Bogoyavlenskiy, Phys. Rev. E **62**, 2158 (2000).
[21] R. Hickling, Phys. Rev. Lett. **73**, 2853 (1994); M.-C. Chu and D. Leung, J. Phys.: Condens. Matter **9**, 3387 (1997); N. Xu, L. Wang, and X. Hu, Phys. Rev. E **57**, 1615 (1998).
[22] V. Vuong, A. Szeri, and D. Young, Phys. Fluids **11**, 10 (1999).
[23] I. Akhatov *et al.*, Phys. Rev. E **55**, 3747 (1997).
[24] A. Prosperetti, Q. Appl. Math. **34**, 339 (1977).
[25] M. Fyrillas and A. Szeri, J. Fluid Mech. **277**, 381 (1994).